Int J Appl Earth Obs Geoinformation 63 (2017) 104–111

Contents lists available at ScienceDirect

Int J Appl Earth Obs Geoinformation

journal homepage: www.elsevier.com/locate/jag

Updating Landsat time series of surface-reflectance composites and forest change products with new observations

Txomin Hermosilla[a,*], Michael A. Wulder[b], Joanne C. White[b], Nicholas C. Coops[a], Geordie W. Hobart[b]

[a] Integrated Remote Sensing Studio, Department of Forest Resources Management, University of British Columbia, 2424 Main Mall, Vancouver, BC, V6T 1Z4, Canada
[b] Canadian Forest Service (Pacific Forestry Centre), Natural Resources Canada, 506 West Burnside Road, Victoria, BC, V8Z 1M5, Canada

ARTICLE INFO

Keywords:
Monitoring
Change detection
Image compositing
Forest
Landsat

ABSTRACT

The use of time series satellite data allows for the temporally dense, systematic, transparent, and synoptic capture of land dynamics over time. Subsequent to the opening of the Landsat archive, several time series approaches for characterizing landscape change have been developed, often representing a particular analytical time window. The information richness and widespread utility of these time series data have created a need to maintain the currency of time series information via the addition of new data, as it becomes available. When an existing time series is temporally extended, it is critical that previously generated change information remains consistent, thereby not altering reported change statistics or science outcomes based on that change information. In this research, we investigate the impacts and implications of adding additional years to an existing 29-year annual Landsat time series for forest change. To do so, we undertook a spatially explicit comparison of the 29 overlapping years of a time series representing 1984–2012, with a time series representing 1984–2016. Surface reflectance values, and presence, year, and type of change were compared. We found that the addition of years to extend the time series had minimal effect on the annual surface reflectance composites, with slight band-specific differences ($r \geq 0.1$) in the final years of the original time series being updated. The area of stand replacing disturbances and determination of change year are virtually unchanged for the overlapping period between the two time-series products. Over the overlapping temporal period (1984–2012), the total area of change differs by 0.53%, equating to an annual difference in change area of 0.019%. Overall, the spatial and temporal agreement of the changes detected by both time series was 96%. Further, our findings suggest that the entire pre-existing historic time series does not need to be re-processed during the update process. Critically, given the time series change detection and update approach followed here, science outcomes or reports representing one temporal epoch can be considered stable and will not be altered when a time series is updated with newly available data.

1. Introduction

Enabled by free and open access to Landsat data in an analysis-ready form (Wulder et al., 2012; Wulder and Coops, 2014), a number of projects have been implemented to inform on the historic dynamics of terrestrial ecosystems over a range of spatial scales, from regional to global (Hansen et al., 2013; Pekel et al., 2016; Potapov et al., 2015). While the amount and distribution of Landsat data in the United States Geological Survey (USGS) Landsat archive is regionally and temporally variable (Wulder et al., 2016), time series methods have evolved to conform to archival data availability (Senf et al., 2015). At present, there are two Landsat satellites in orbit collecting a combined ~1200 images per day for ingest to the USGS archive (Wulder et al., 2016). Furthermore, there are measures from compatible sensors (such as Sentinel-2; Drusch et al., 2012) that have spatial and spectral complementarity enabling integration with Landsat data (Wulder et al., 2015). Robust cross-sensor calibration has enabled the compatibility of the various Landsat data streams through time (Markham and Helder, 2012; Roy et al., 2015), and continuous Landsat acquisitions allow for the extension of previously produced time series, allowing new measures of the Earth's surface to be ingested and integrated on an ongoing basis.

Leveraging the available Landsat archive in a transparent, systematic, and repeatable manner, several algorithms have been developed to characterize landscape change. These algorithms are no longer hindered by data costs; however, processing requirements can be notable (Hansen et al., 2013; Hermosilla et al., 2016; Sexton et al., 2013). Several studies have demonstrated the capacity to exhaustively portray

* Corresponding author.
E-mail addresses: txomin.hermosilla@ubc.ca, txominhermos@gmail.com (T. Hermosilla).

http://dx.doi.org/10.1016/j.jag.2017.07.013
Received 28 June 2017; Received in revised form 26 July 2017; Accepted 30 July 2017
Available online 05 August 2017

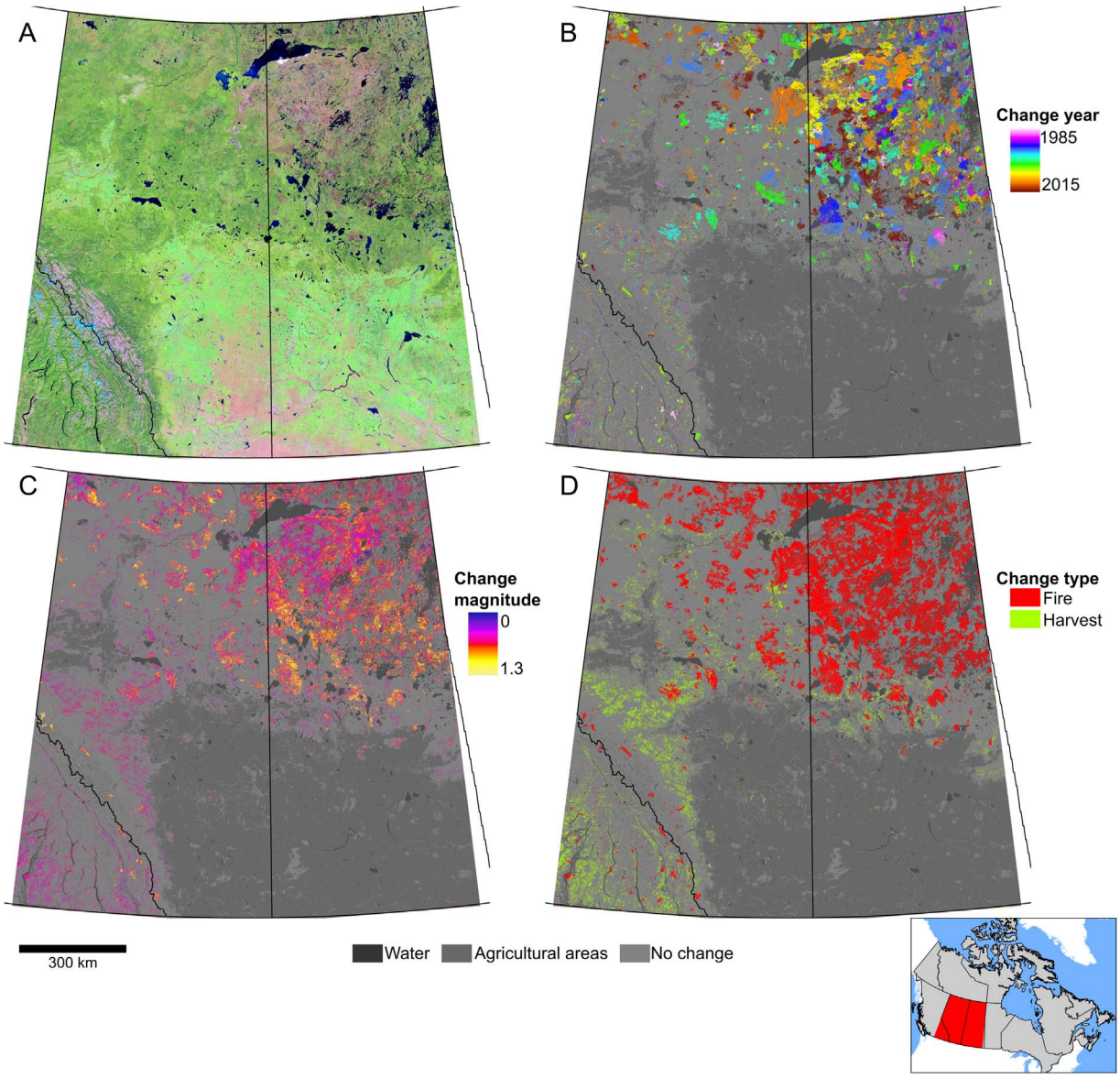

Fig. 1. (A) False color (bands: SWIR-1-NIR-R) proxy image composite in 2016, (B) changes by year, (C) change magnitude, and (D) change types in the study area. The complete study area is highlighted in the map inset.

large areas with Landsat image composites, combining pixels from multiple images according to a pre-defined rule set (Griffiths et al., 2013; Roy et al., 2010; White et al., 2014), and augmented with synthetic surface reflectance values to address situations when no pixel value meets phenological and/or atmospheric clarity constraints (Hermosilla et al., 2015a; Zhu et al., 2015). Access to the entirety of the Landsat archive has likewise promoted temporal analysis approaches of spectral trends for change detection (Huang et al., 2010; Kennedy et al., 2010; Verbesselt et al., 2010; Zhu et al., 2012), as well as automated approaches for attributing change to a particular change type (Hermosilla et al., 2015b; Schroeder et al., 2017).

Time series change algorithms can capture a broader range of forest change types than was previously possible with bi-temporal change detection approaches, including spatially and temporally discrete changes such as wildfire and harvest, as well as more gradual, amorphous changes such as stress, disease, or defoliation (Hughes et al., 2017; Kennedy et al., 2014; Vogelmann et al., 2016). The ability to attribute to change type allows for better understanding of drivers of change, such as ecosystem stress (e.g., Cohen et al., 2016) and forest management (White et al., 2017), or to inform models requiring parametrization of post-change, disturbance type-specific recovery trajectories (Williams et al., 2014). The variety of Landsat time series algorithms now available has lead an interest in learning more about the relative capacities of these algorithms for detecting change (Cohen et al., 2017) with the variably in mapped outcomes linked to both the nature of the disturbance and the particulars of the algorithm applied. Importantly, the year-on-year information from time series analysis of imagery provides additional trend information that allows for strengthening of models (Pflugmacher et al., 2012) and incorporation of ecological insights and successional expectations for mapping land cover (Gómez et al., 2016).

Common to most approaches involving Landsat time series is the description of spectral trends and the detection of change events via an analysis of a complete temporal sequence (Hughes et al., 2017; Zhu, 2017). Keeping composited imagery and associated derivatives (i.e., metrics; Hermosilla et al., 2015b; Pflugmacher et al., 2012) up-to-date involves the addition of new data to the end of the time series. The addition of these new data, however, may result in changes to spectral trends, which are determined through the identification of spectral breakpoints and fitting of linear segments to capture the spectral

Table 1
Characteristics of the coincident bands for the Landsat sensors.

Name	TM		ETM+		OLI	
	Band	Wavelength (μm)	Band	Wavelength (μm)	Band	Wavelength (μm)
Blue (B)	1	0.45–0.52	1	0.45–0.52	2	0.45–0.51
Green (G)	2	0.52–0.60	2	0.52–0.60	3	0.53–0.59
Red (R)	3	0.63–0.69	3	0.63–0.69	4	0.64–0.67
Near Infrared (NIR)	4	0.76–0.90	4	0.77–0.90	5	0.85–0.88
Shortwave Infrared (SWIR) 1	5	1.55–1.75	5	1.55–1.75	6	1.57–1.65
Shortwave Infrared (SWIR) 2	7	2.08–2.35	7	2.09–2.35	7	2.11–2.29

trajectories (Hermosilla et al., 2015a; Kennedy et al., 2010). These different trends, in turn, may alter derived image composites and change detection outputs, particularly at the temporal junction between new and existing data. It is important that scientists, managers, and policy makers have confidence that the outcomes derived from a given image time series data set are stable and not subject to notable variability upon addition of more recent data and related reprocessing. For instance, confidence in forest monitoring programs would be undermined if previously reported statistical information required frequent, data-related revision. Thus, the objective of this study is to demonstrate the capacity and identify potential challenges associated with the addition of new observations to an existing Landsat time series for the purposes of updating forest change information. We build upon the image compositing and spectral trend analysis methods presented in the Composite2Change (C2C) approach representing 1984–2012 (hereafter, $C2C_{84\text{-}12}$; Hermosilla et al., 2016). We add new Landsat observations representing the four years from 2013 to 2016 (corresponding with the launch of Landsat-8 OLI) to the time series to update seamless annual surface-reflectance image composites and attributed forest change outputs ($C2C_{84\text{-}16}$). We compare the overlapping years of image composites and attributed change products from $C2C_{84\text{-}12}$ with those from $C2C_{84\text{-}16}$ and report on the spectral, spatial, and categorical differences between both products in order to determine the implications of adding new data to extend a given Landsat time series and associated outputs (i.e., change products).

2. Study area

The study area is approximately 143 Mha and occupies three UTM zones (11–13) as intersecting portions of the Canadian provinces of Alberta, Saskatchewan, and British Columbia (Fig. 1). This area was selected to represent a range of natural and anthropogenic disturbances of variable size, distribution, and magnitude. The southern portions of the study area are comprised by the Prairies on the east (dominated by extensive agriculture, wetlands, and grasslands), and by the Montane Cordillera to the west (encompassing the Alberta Foothills and the interior mountain ranges of British Columbia). The northern portion of the study area is comprised of four forested ecozones, including the Boreal Plains, Boreal Shield, Taiga Plains, and Taiga Shield (Rowe, 1996). The vegetation of the northern forested ecozones is primarily composed of black spruce (*Picea mariana*) and Jack pine (*Pinus banksiana*). These northern forest areas are largely unmanaged, with no commercial tenures for harvesting and limited fire suppression activities (Brandt et al., 2013) and wildfires are the main disturbance agent (Kurz and Apps, 1999; White et al., 2017). The more southern reaches of the forested ecosystems are dominated by aspen (*Populus tremuloides*), white spruce (*Picea glauca*), and tamarack (*Larix laricina*), and are subject to sustainable forest management activities (including fire suppression) with ongoing tenure arrangements allowing for timber harvest (Wulder et al., 2004).

3. Methods

3.1. Data

Image composites were generated using all available images with cloud cover less than 70% from the United States Geological Survey (USGS) archive of Level-1-Terrain-Corrected (L1T) Landsat-4 and −5 Thematic Mapper (TM), Landsat-7 Enhanced Thematic Mapper Plus (ETM+) and Landsat-8 Operational Land Imager (OLI) covering the study area. The eligible date range for candidate images was August 1st ± 30 days from 1984 to 2016. August 1st was selected as central target date due to a correspondence with the growing season for the majority of Canada's forested ecosystems (McKenney et al., 2006). Images were corrected to surface reflectance using the LEDAPS algorithm (Masek et al., 2006; Schmidt et al., 2013). The characteristics of the coincident bands for the different Landsat sensors are shown in Table 1 (Roy et al., 2016). The study area was comprised of 285 scenes (path/rows) of the Landsat Worldwide Referencing System (WRS-2). A total of 17,200 images met the inclusion criteria, from which 14,567 images were ultimately used to create the image composites (Fig. 2). Note that the 2013 launch of Landsat-8 OLI (Roy et al., 2014) coincides with a high, multi-sensor image yield, and with the beginning of our four year (2013–2016) update period.

3.2. Composite2Change (C2C) approach

Annual gap-free, seamless, Landsat surface reflectance composites and 30-m forest change products were generated following the Composite2Change (C2C) approach (Hermosilla et al., 2016). The C2C approach is based on annual best-available pixel (BAP) image composites generated from Landsat imagery by selecting the most suitable observations for each pixel location from all the candidate images acquired within a specific date range (August 1 ± 30 days) and following the scoring functions defined by (White et al., 2014). These functions rank every pixel based on the presence and distance to clouds and their shadows (detected by the Fmask algorithm, Zhu and

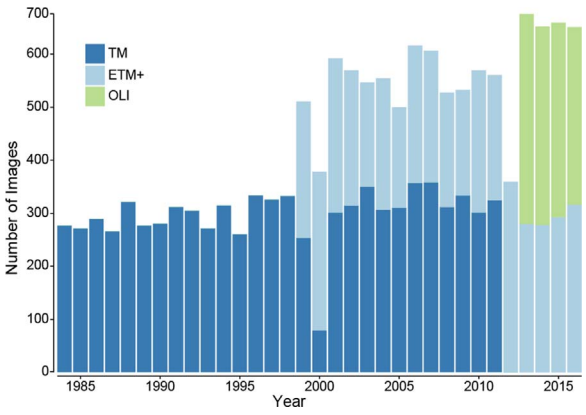

Fig. 2. Number of images used to create the image composites by year and sensor.

Woodcock, 2012; Zhu and Woodcock 2014), atmospheric quality, and acquisition sensor. The acquisition sensor score (see Hermosilla et al., 2016) prioritized Landsat TM (until 2012) and OLI (since 2013) data over ETM+ due to the scan line corrector failure (SLC-off, i.e. after 31 May 2003).

The annual BAP image composites were further refined by removing noisy (e.g., residual cloud/shadow, smoke, haze) observations (Kennedy et al., 2010) and infilling data gaps with proxy surface reflectance values using spectral trend analysis of pixel time series (Hermosilla et al., 2015a). Temporal trends and changes were detected using a bottom-up breakpoint detection algorithm (Keogh et al., 2001) applied to Normalized Burn Ratio (NBR) values (Key and Benson, 2006). This algorithm first divided the time series composed by n elements into n-1 segments for every pixel. The cost of merging each pair of adjacent segments was then computed using the Root-Mean-Square Error (RMSE), and the pair with the lowest cost was merged. The cost value was recomputed for the new segments and the process is iterated until the maximum number of segments are used. For the analysis of the original time series (i.e. $C2C_{84\text{-}12}$) a maximum of five segments to be fitted was defined for change detection (noting that changes are not detected in the first and last year of the time series). Given the longer time span considered in extended time series ($C2C_{84\text{-}16}$), and in order to enable the detection of overlapping change events, we defined a maximum of six segments. From these trends, we derived a set of descriptive change metrics that allowed us to characterize the change events, including the change magnitude, defined as the difference between NBR values after and before the change event. Finally, the detected changes were attributed to a change type (with special focus on fire and harvesting; White et al., 2017), based on their spectral, temporal, and geometrical characteristics using a Random Forests model and following the object-based image analysis approach presented in (Hermosilla et al., 2015b). Stand replacing disturbances, such as harvest and wildfire, are commonly mapped using Landsat time series although not frequently labeled. The high magnitude nature of the difference in pre- and post-disturbance condition results in reliable and consistent capture of these stand-replacing disturbances. With the number of votes received by each change class we also defined an indicator of attribution confidence using the ratio between the percentage of votes of the second most voted class and the percentage of votes of the attributed (most voted) class (Hermosilla et al., 2016; Mitchell et al., 2008). This indicator of attribution confidence allowed us to distinguish between change types attributed with a high confidence (ratio $>$ 0.4) versus those with a low confidence (ratio $\leq$ 0.4). The labeling of disturbance to type is focused on categories expected over forested ecosystems, and therefore agricultural lands were identified and excluded from labelling procedures using a mask provided by Agriculture and Agri-Foods Canada (2011 data).[1]

3.3. Assessment of the time series extension

We assessed the impact of adding new data to the time series at spectral and temporal levels, corresponding to the two key outputs of C2C approach: seamless (gap-free) surface-reflectance image composites and forest change information products. Spectrally, the proxy values of the surface-reflectance image composites were compared using the Pearson's correlation coefficient between $C2C_{84\text{-}12}$ and $C2C_{84\text{-}16}$ for every band and for years common to both time series (1984–2012). To enable the comparison, a random sample of 50,000 pixels with proxy surface reflectance values that were located in forested land areas (i.e., water and agricultural lands were excluded) were selected from each year and band of the overlapping period.

For the assessment of the forest-change products, we compared the C2C change output (i.e. both fire and harvesting). We used indicators that summarized the various cases of spatio-temporal overlap (1985–2011) between changes detected by the original $C2C_{84\text{-}12}$ and the extended $C2C_{84\text{-}16}$ time series, including spatio-temporal coincidence, temporal difference, and omission and commission errors. Coincidence refers to changes detected by both the original and extended time series that spatially correspond and that are labelled to the same year. Temporal difference represents pixels detected as change by both original and extended time series that spatially correspond but that were detected in different years. Omission refers to those pixels detected as change by the original time series that are not detected as change in $C2C_{84\text{-}16}$. Conversely, commission represents pixels that are not defined as change in the original time series, but are detected as change in $C2C_{84\text{-}16}$. Distances between pixels identified as either omission or commission in $C2C_{84\text{-}16}$ and change pixels identified in $C2C_{84\text{-}12}$ were also computed and reported. We report results by change type (i.e., fire and harvesting; Hermosilla et al., 2015b) and change magnitude in order to explore any possible impacts that extending the time series may have on C2C's capacity to model change type.

4. Results

4.1. Spectral assessment

The Pearson's correlation coefficients resulting from the comparison of a sample of proxy surface-reflectance values for $C2C_{84\text{-}12}$ and $C2C_{84\text{-}16}$ for each band and each year are summarized in Fig. 3. For the majority of years, $r = 1$ for all bands. Generally, correlations between proxy values from the two time series decreased after 2001, with 2012 having the lowest correlations. Bands of the SWIR region were less impacted than bands in the visible and NIR. The lowest correlation values ($r = 0.86$) were found for the green and NIR bands in 2012.

4.2. Change detection and attribution assessment

The total area of change estimated during the overlapping period (1985–2011) of forest change information for $C2C_{84\text{-}12}$ and $C2C_{84\text{-}16}$ is presented in Table 2, stratified by change type and attribution confidence. Overall, the area estimated by the $C2C_{84\text{-}16}$ time series for stand replacing change was slightly larger (0.53%) than $C2C_{84\text{-}12}$, or an average difference of 0.019% per year. As expected, a greater similarity in change area is found for the high confidence attributions (0.08%), compared to low confidence attributions (7.29%). When further considered by change type, the area impacted by fire had the greatest similarity in change area between the original and extended time series, differing by 0.04% overall. $C2C_{84\text{-}16}$ had less high confidence fire (-0.75%), but also more area identified as low confidence fire (17.79%). By comparison, $C2C_{84\text{-}16}$ estimated 3.30% more high confidence harvested area and 4.81% less low confidence harvest area. In summary, the extended time series resulted in an increase in estimated aggregate change area; however, on an annual basis, this increase is small relative to the size of the study area (143 Mha) and when considered by year. For stand replacing changes (considering both high and low confidence attributions), $C2C_{84\text{-}16}$ estimated approximately 2722 ha yr^{-1} more change area: 177 ha yr^{-1} for fire and 2544 ha yr^{-1} for harvest.

Table 3 summarizes the results of the spatial overlap assessment between changes detected by $C2C_{84\text{-}12}$ and $C2C_{84\text{-}16}$ for the temporally overlapping period, expressed as a proportion of the pixels identified as change in $C2C_{84\text{-}12}$. Overall, there was a high level of spatial correspondence between the changes detected by both time series. Fire had the greatest spatial coincidence, with 97.2% of pixels identified as fire in $C2C_{84\text{-}12}$ also identified as fire in $C2C_{84\text{-}16}$ (in the same year). Only 0.4% of pixels identified as fire in $C2C_{84\text{-}12}$ were identified as fire in a different year in $C2C_{84\text{-}16}$, and only 3.6% of $C2C_{84\text{-}12}$ fire pixels were not detected as fire in $C2C_{84\text{-}16}$. $C2C_{84\text{-}16}$ identified 2.4% more pixels as fire compared to $C2C_{84\text{-}12}$. For harvest, spatial coincidence was lower

[1] //ftp.agr.gc.ca/pub/outgoing/aesb-eos-gg/CEN_CA_AG_INTRP/AgrMask2011/AgriculturalMask2011_AAFC.gdb.zip.

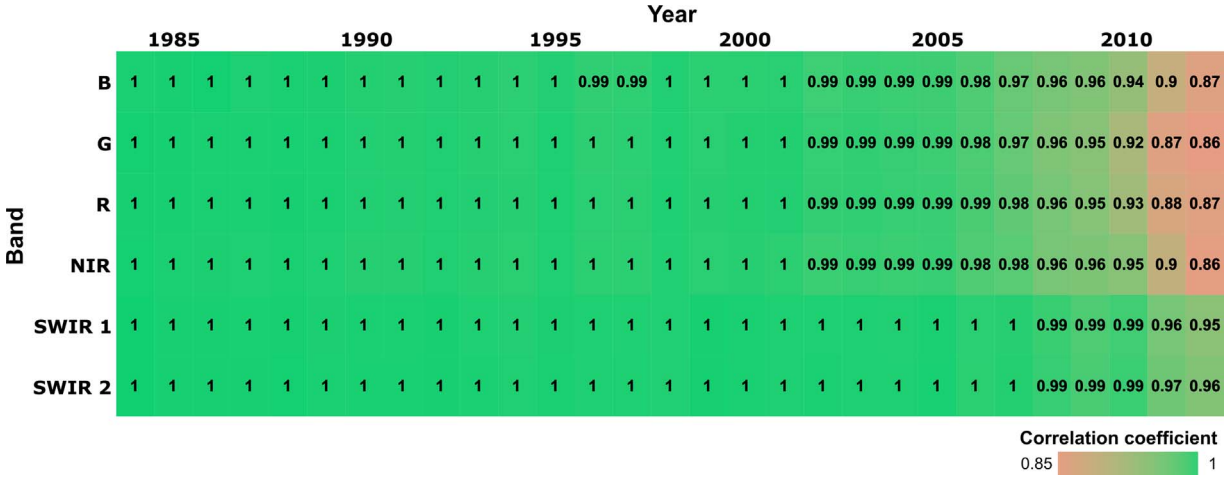

Fig. 3. Pearson's correlation coefficient values for a sample of proxy surface reflectance values from the overlapping years (1984–2012) of the original $C2C_{84\text{-}12}$ and extended $C2C_{84\text{-}16}$ time series. Landsat band characteristics are summarized in Table 1.

Table 2
Comparison of area detected as changed by $C2C_{84\text{-}12}$ and $C2C_{84\text{-}16}$ grouped by attribution confidence (conf.).

	$C2C_{84\text{-}12}$(ha)			$C2C_{84\text{-}16}$(ha)			Relative difference (%)		
	High conf.	Low conf.	All	High conf.	Low conf.	All	High conf.	Low conf.	All
Fire	10,308,968	460,342	10,769,310	10,231,878	542,234	10,774,112	−0.75	17.79	0.04
Harvesting	2,661,532	399,547	3,061,079	2,749,451	380,321	3,129,772	3.30	−4.81	2.24
Total	**12,970,500**	**859,889**	**13,830,389**	**12,981,329**	**922,555**	**13,903,884**	**0.08**	**7.29**	**0.53**

Table 3
Assessment of changes detected by $C2C_{84\text{-}12}$ and $C2C_{84\text{-}16}$ expressed as proportion of the changes in $C2C_{84\text{-}12}$.

Type	Coincidence	Temporal difference	Omission	Commission
Fire	97.2%	0.4%	2.4%	2.4%
Harvesting	90%	0.8%	9.2	11.5%
Total	96%	0.5%	3.6	4.1%

(90%), with approximately 0.8% of pixels identified as harvest in a different year. Omissions were also greater for harvest, with 9.2% of pixels identified as harvest in $C2C_{84\text{-}12}$ not identified as harvest in $C2C_{84\text{-}16}$. Of note, $C2C_{84\text{-}16}$ identified 11.5% more pixels as fire compared to $C2C_{84\text{-}12}$. Examples of these results are spatially displayed in Fig. 4.

To better understand the nature of the omission and commission trends present, we calculated the distance, in pixels, between those pixels identified as omission or commission in $C2C_{84\text{-}16}$ and change pixels identified in $C2C_{84\text{-}12}$ (Table 4). The omission and commission errors for fire and harvesting have respectively 90.5% and 84.7% of the pixels labelled differently within a 2-pixel distance of identified pixels in $C2C_{84\text{-}12}$. This result suggests that for the majority of stand replacing disturbance, omission or commission errors are concentrated around the periphery of changes identified in $C2C_{84\text{-}12}$ (i.e. fire in Fig. 4a and harvesting in Fig. 4b).

The distribution of the change magnitude metric for the four spatial overlap assessment cases is presented in a boxplot in Fig. 5. Coincident pixels displayed the largest variation in change magnitude, whereas omission and commission cases had the smallest change magnitude. Changes detected but labelled in different dates comprised pixels with moderate change magnitude values.

5. Discussion

In this research, we assessed the impact of adding new data to the end of an existing time series to extend the temporal sequence of Landsat surface-reflectance composites (White et al., 2014) and forest change products (Hermosilla et al., 2015b) generated using the C2C protocol (Hermosilla et al., 2016). The addition of new observations to a time series may require the adaptation of processing approaches if new image sources are incorporated (e.g. Landsat-8 OLI), or if algorithm-specific parameters require adjustment to accommodate a longer time period. In our case, we increased the maximum number of change segments (Kennedy et al., 2010) to be used in the C2C spectral trend analysis (from five to six segments), since additional observations extended the temporal analysis period and increased the likelihood of multiple change events for a given pixel. Our results indicated a slight decrease in the level of correlation between $C2C_{84\text{-}12}$ and $C2C_{84\text{-}16}$ proxy surface reflectance values, particularly after 2001 for the visible and NIR bands. We also found that extending the time series resulted in a small increase (0.53%) in the estimated area of stand replacing change over the period analyzed. Overall, these results indicate that the C2C approach is robust to the addition of new observations for extension of the time series and is capable of producing consistent image composites and stand replacing change products.

Differences in the proxy surface reflectance values between the original ($C2C_{84\text{-}12}$) and extended ($C2C_{84\text{-}16}$) time series image composites occur primarily in the later years of the common period analyzed. This outcome is logical given that the proxy values were informed by the additional observations added to the time series (4 more years). Moreover, the image composites representing 2013–2016 were created using Landsat-8 OLI imagery, which is acquiring more data relative to previous Landsat sensors (Wulder et al., 2016), thereby enabling more complete image composites with fewer data gaps. The lowest correlations (i.e. $r \leq 0.9$) between the original and extended time series, were found in the last two years of the common period, and impacted the visible and NIR bands. This is likely caused by the larger impact of atmospheric effects on the shorter spectral wavelengths than on the Landsat bands located in the mid-infrared (Liang et al., 2002). Further, the slight differences in spectral band correspondences (Roy et al.,

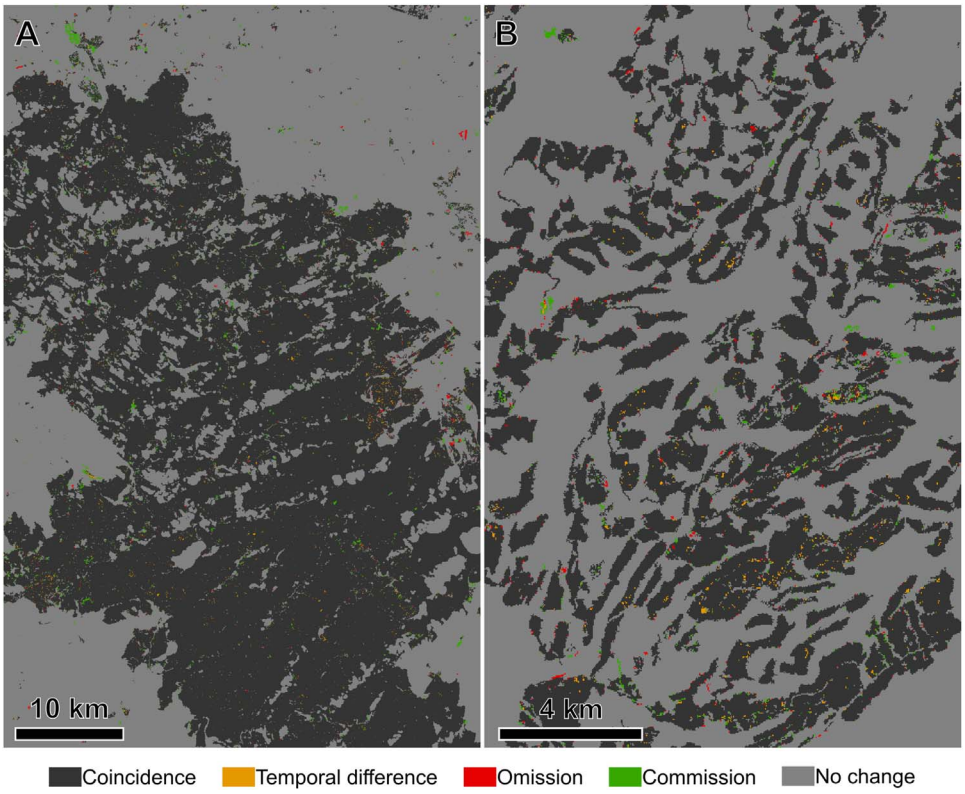

Fig. 4. Examples of spatial distribution of the overlap assessment cases in areas dominated by (a) fires and (b) harvesting.

Table 4
Relative frequency of distance to coincidence cases for omissions and commissions per change type.

Distance (pixels)	Fire (%)	Harvest (%)
1	80.8	73.8
2	9.7	10.9
3	3.2	4.1
4	1.7	2.3
≥5	4.6	8.9

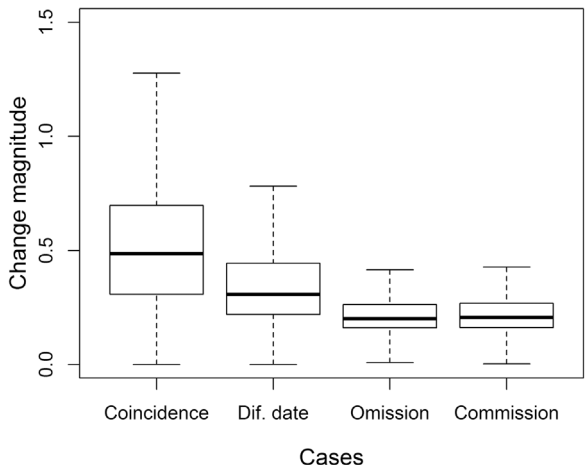

Fig. 5. Boxplot representing median, interquartile range, and extreme values for change magnitude metric across the spatial overlap assessment cases.

2016) between Landsat-8 OLI and Landsats-5 TM and -7 ETM+ (Table 1) may also have an impact upon correlations (via the segment-based breakpoint detection and proxy value calculation). The operational implications of these results suggest that adding more years to extend a time series of image composites does not necessarily require fully re-processing all years. The amount of overlapping years of the original series to be re-process would range between 20% (6 years) when $r < 0.98$ is consider, and 38% (11 years) in a more conservative approach ($r < 1$).

The forest stand replacing changes determined with both original and extended series presented high spatial and temporal agreement, with the differences associated with lower magnitude changes. The pixel-to-pixel differences were concentrated around the perimeter of changes identified in $C2C_{84\text{-}12}$, indicating that the same change events (objects) are detected and attributed, but slightly differently delineated. Overall, commission, or the identification of more change in the $C2C_{84\text{-}16}$ time series, was greater than omission. This is likely a product of using a larger number segments to perform the spectral trend analysis; however, the increase in change area is minimal when considered on an annual basis: 0.08% for harvesting and 0.002% for fire. The stability and consistency in the outcomes are key findings, since stand replacing changes (i.e., fire, and harvesting) are critical for forest monitoring and reporting activities, in addition to applications including carbon budgets, biodiversity assessments, and habitat characterizations.

6. Conclusions

Keeping satellite-derived land cover and land cover change datasets up-to-date requires periodic integration of newly acquired data. The update process involves adapting and modifying algorithms and protocols that may entail differences to previously generated (and reported) datasets. We have analyzed the integration of Landsat-8 OLI data to extend the period depicted by the seamless surface reflectance composites and forest change products produced with the C2C protocol (Hermosilla et al., 2016). This study demonstrated that adding new data to extend the time series has a minimal impact on the annual proxy surface reflectance composites, with some differences ($r \geq 0.1$) in the later years of the time series primarily in the visible and NIR wavelengths. Moreover, the use of an additional temporal segment in the in the trend analysis does not substantially alter the stand replacing

change results, either spatially (change vs. no change), or temporally (i.e., year of detection). Notably, the subsequent modeled attribution of the detected changes to a disturbance agent (i.e., fire, harvesting) does not change markedly. These results suggest that economies of scale are possible in an operational context, whereby additional years can be added to extend the time series with a limited number of overlapping years (between six and eleven years) requiring reprocessing. This would limit the computational effort required, as the entire time series data would not need to be fully reprocessed every time new data are added in order to maintain up-to-date satellite-based land cover monitoring products.

Acknowledgments

This research was undertaken as part of the "National Terrestrial Ecosystem Monitoring System (NTEMS): Timely and detailed national cross-sector monitoring for Canada" project jointly funded by the Canadian Space Agency (CSA), Government Related Initiatives Program (GRIP), and the Canadian Forest Service (CFS) of Natural Resources Canada. This research was enabled in part by support provided by WestGrid (www.westgrid.ca) and Compute Canada (www.computecanada.ca). We appreciate the time, effort, and insight offered by the journal editors and reviewers.

References

Brandt, J.P., Flannigan, M.D., Maynard, D.G., 2013. An introduction to Canada's boreal zone: ecosystem processes, health, sustainability, and environmental. Environ. Rev. 226 (1), 207–226.

Cohen, W.B., Yang, Z., Stehman, S.V., Schroeder, T.A., Bell, D.M., Masek, J.G., Huang, C., Meigs, G.W., 2016. Forest disturbance across the conterminous United States from 1985 to 2012: the emerging dominance of forest decline. For. Ecol. Manage. 360, 242–252. http://dx.doi.org/10.1016/j.foreco.2015.10.042.

Cohen, W.B., Healey, S.P., Yang, Z., Stehman, S.V., Brewer, C.K., Brooks, E.B., Gorelick, N., Huang, C., Hughes, M.J., Kennedy, R.E., Loveland, T.R., Moisen, G.G., Schroeder, T.A., Vogelmann, J.E., Woodcock, C.E., Yang, L., Zhu, Z., 2017. How similar are forest disturbance maps derived from different Landsat time series algorithms? Forests 8, 1–19. http://dx.doi.org/10.3390/f8040098.

Drusch, M., Del Bello, U., Carlier, S., Colin, O., Fernandez, V., Gascon, F., Hoersch, B., Isola, C., Laberinti, P., Martimort, P., Meygret, a., Spoto, F., Sy, O., Marchese, F., Bargellini, P., 2012. Sentinel-2: ESA's optical high-resolution mission for GMES operational services. Remote Sens. Environ. 120, 25–36. http://dx.doi.org/10.1016/j.rse.2011.11.026.

Gómez, C., White, J.C., Wulder, M.A., 2016. Optical remotely sensed time series data for land cover classification: a review. ISPRS J. Photogramm. Remote Sens. 116, 55–72. http://dx.doi.org/10.1016/j.isprsjprs.2016.03.008.

Griffiths, P., Van Der, Linden S., Kuemmerle, T., Hostert, P., 2013. A pixel-based Landsat compositing algorithm for large area land cover mapping. IEEE J. Sel. Top. Appl. Earth Obs. Remote Sens. 6, 2088–2101.

Hansen, M.C., Potapov, P.V., Moore, R., Hancher, M., Turubanova, S.A., Tyukavina, A., Thau, A., Stehman, S.V., Goetz, S.J., Loveland, T.R., Kommareddy, A., Egorov, A., Chini, L., Justice, C.O., Townshend, J.R.G., 2013. High-resolution global maps of 21st-century forest cover change. Science 342, 850–853. http://dx.doi.org/10.1126/science.1244693.

Hermosilla, T., Wulder, M.A., White, J.C., Coops, N.C., Hobart, G.W., 2015a. An integrated Landsat time series protocol for change detection and generation of annual gap-free surface reflectance composites. Remote Sens. Environ. 158, 220–234. http://dx.doi.org/10.1016/j.rse.2014.11.005.

Hermosilla, T., Wulder, M.A., White, J.C., Coops, N.C., Hobart, G.W., 2015b. Regional detection, characterization, and attribution of annual forest change from 1984 to 2012 using Landsat-derived time-series metrics. Remote Sens. Environ. 170, 121–132. http://dx.doi.org/10.1016/j.rse.2015.09.004.

Hermosilla, T., Wulder, M.A., White, J.C., Coops, N.C., Hobart, G.W., Campbell, L.B., 2016. Mass data processing of time series Landsat imagery: pixels to data products for forest monitoring. Int. J. Digit. Earth 9, 1035–1054. http://dx.doi.org/10.1080/17538947.2016.1187673.

Huang, C., Goward, S.N., Masek, J.G., Thomas, N., Zhu, Z., Vogelmann, J.E., 2010. An automated approach for reconstructing recent forest disturbance history using dense Landsat time series stacks. Remote Sens. Environ. 114, 183–198. http://dx.doi.org/10.1016/j.rse.2009.08.017.

Hughes, M., Kaylor, S., Hayes, D., 2017. Patch-based forest change detection from Landsat time series. Forests 8, 166. http://dx.doi.org/10.3390/f8050166.

Kennedy, R.E., Yang, Z., Cohen, W.B., 2010. Detecting trends in forest disturbance and recovery using yearly Landsat time series: 1. LandTrendr—Temporal segmentation algorithms. Remote Sens. Environ. 114, 2897–2910. http://dx.doi.org/10.1016/j.rse.2010.07.008.

Kennedy, R.E., Andréfouët, S., Cohen, W.B., Gómez, C., Griffiths, P., Hais, M., Healey, S.P., Helmer, E.H., Hostert, P., Lyons, M.B., Meigs, G.W., Pflugmacher, D., Phinn, S.R., Powell, S.L., Scarth, P., Sen, S., Schroeder, T.A., Schneider, A., Sonnenschein, R., Vogelmann, J.E., Wulder, M.A., Zhu, Z., 2014. Bringing an ecological view of change to Landsat-based remote sensing. Front. Ecol. Environ. 12, 339–346. http://dx.doi.org/10.1890/130066.

Keogh, E., Chu, S., Hart, D., Pazzani, M., 2001. An online algorithm for segmenting time series. In: Data Mining, 2001. ICDM, Proceedings IEEE International Conference on. IEEE Comput. Soc, San Jose, CA. pp. 289–296. http://dx.doi.org/10.1109/ICDM.2001.989531.

Key, C.H., Benson, N.C., 2006. Landscape assessment (LA): Sampling and analysis methods. USDA For. Serv. Gen. Tech. Rep. RMRS-GTR-164-CD.

Kurz, W.A., Apps, M.J., 1999. A 70-year retrospective analysis of carbon fluxes in the Canadian Forest Sector. Ecol. Appl. 9, 526–547. http://dx.doi.org/10.1890/1051-0761(1999)009[0526:AYRAOC]2.0.CO;2.

Liang, S., Fang, H., Morisette, J.T., 2002. Atmospheric correction of Landsat ETM+ land surface imagery. II. Validation and applications. IEEE Trans. Geosci. Remote Sens. 40, 2736–2746. http://dx.doi.org/10.1109/tgrs.2002.807579.

Markham, B.L., Helder, D.L., 2012. Forty-year calibrated record of earth-reflected radiance from Landsat: a review. Remote Sens. Environ. 122, 30–40. http://dx.doi.org/10.1016/j.rse.2011.06.026.

Masek, J.G., Vermote, E.F., Saleous, N.E., Wolfe, R., Hall, F.G., Huemmrich, K.F., Gao, F., Kutler, J., Lim, T.K., 2006. A Landsat surface reflectance dataset for North America, 1990–2000. Geosci. Remote Sens. Lett. IEEE 3, 68–72.

McKenney, D., Pedlar, J., Papadopol, P., Hutchinson, M., 2006. The development of 1901–2000 historical monthly climate models for Canada and the United States. Agric. For. 138, 69–81. http://dx.doi.org/10.1016/j.agrformet.2006.03.012.

Mitchell, S.W., Remmel, T.K., Csillag, F., Wulder, M.A., 2008. Distance to second cluster as a measure of classification confidence. Remote Sens. Environ. 112, 2615–2626. http://dx.doi.org/10.1016/j.rse.2007.12.006.

Pekel, J.-F., Cottam, A., Gorelick, N., Belward, A.S., 2016. High-resolution mapping of global surface water and its long-term changes. Nature 540, 1–19. http://dx.doi.org/10.1038/nature20584.

Pflugmacher, D., Cohen, W.B., Kennedy, R., 2012. Using Landsat-derived disturbance history (1972–2010) to predict current forest structure. Remote Sens. Environ. 122, 146–165. http://dx.doi.org/10.1016/j.rse.2011.09.025.

Potapov, P.V., Turubanova, S.A., Tyukavina, A., Krylov, A.M., McCarty, J.L., Radeloff, V.C., Hansen, M.C., 2015. Eastern Europe's forest cover dynamics from 1985 to 2012 quantified from the full Landsat archive. Remote Sens. Environ. 159, 28–43. http://dx.doi.org/10.1016/j.rse.2014.11.027.

Rowe, J.S., 1996. Land classification and ecosystem classification. Environ. Monit. Assess. 39, 11–20. http://dx.doi.org/10.1007/BF00396131.

Roy, D.P., Ju, J., Kline, K., Scaramuzza, P.L., Kovalskyy, V., Hansen, M., Loveland, T.R., Vermote, E., Zhang, C., 2010. Web-enabled Landsat data (WELD): Landsat ETM+ composited mosaics of the conterminous United States. Remote Sens. Environ. 114, 35–49. http://dx.doi.org/10.1016/j.rse.2009.08.011.

Roy, D.P., Wulder, M.A., Loveland, T.R., Woodcock, C.E., Allen, R.G., Anderson, M.C., Helder, D., Irons, J.R., Johnson, D.M., Kennedy, R., Scambos, T.A., Schaaf, C.B., Schott, J.R., Sheng, Y., Vermote, E.F., Belward, A.S., Bindschadler, R., Cohen, W.B., Gao, F., Hipple, J.D., Hostert, P., Huntington, J., Justice, C.O., Kilic, A., Kovalskyy, V., Lee, Z.P., Lymburner, L., Masek, J.G., McCorkel, J., Shuai, Y., Trezza, R., Vogelmann, J., Wynne, R.H., Zhu, Z., 2014. Landsat-8: Science and product vision for terrestrial global change research. Remote Sens. Environ. 145, 154–172. http://dx.doi.org/10.1016/j.rse.2014.02.001.

Roy, D.P., Kovalskyy, V., Zhang, H., Yan, L., 2015. The utility of Landsat data for global long term terrestrial monitoring. Remote Sensing Time Series. pp. 289–305. http://dx.doi.org/10.1007/978-3-319-15967-6.

Roy, D.P., Kovalskyy, V., Zhang, H.K., Vermote, E.F., Yan, L., Kumar, S.S., Egorov, A., 2016. Characterization of Landsat-7 to Landsat-8 reflective wavelength and normalized difference vegetation index continuity. Remote Sens. Environ. 185, 57–70. http://dx.doi.org/10.1016/j.rse.2015.12.024.

Schmidt, G.L., Jenkerson, C.B., Masek, J., Vermote, E., Gao, F., 2013. Landsat Ecosystem Disturbance Adaptive Processing System (LEDAPS) Algorithm Description.

Schroeder, T.A., Schleeweis, K.G., Moisen, G.G., Toney, C., Cohen, W.B., Freeman, E.A., Yang, Z., Huang, C., 2017. Testing a Landsat-based approach for mapping disturbance causality in U.S. forests. Remote Sens. Environ. 195, 230–243. http://dx.doi.org/10.1016/j.rse.2017.03.033.

Senf, C., Leitão, P.J., Pflugmacher, D., van der Linden, S., Hostert, P., 2015. Mapping land cover in complex Mediterranean landscapes using Landsat: improved classification accuracies from integrating multi-seasonal and synthetic imagery. Remote Sens. Environ. 156, 527–536. http://dx.doi.org/10.1016/j.rse.2014.10.018.

Sexton, J.O., Song, X.-P., Feng, M., Noojipady, P., Anand, A., Huang, C., Kim, D.-H., Collins, K.M., Channan, S., DiMiceli, C., Townshend, J.R., 2013. Global, 30-m resolution continuous fields of tree cover: Landsat-based rescaling of MODIS vegetation continuous fields with lidar-based estimates of error. Int. J. Digit. Earth 6, 427–448. http://dx.doi.org/10.1080/17538947.2013.786146.

Verbesselt, J., Hyndman, R., Zeileis, A., Culvenor, D.S., Newnham, G.J., 2010. Detecting trend and seasonal changes in satellite image time series. Remote Sens. Environ. 114, 106–115. http://dx.doi.org/10.1016/j.rse.2010.08.003.

Vogelmann, J.E., Gallant, A.L., Shi, H., Zhu, Z., 2016. Perspectives on monitoring gradual change across the continuity of Landsat sensors using time-series data. Remote Sens. Environ. 185, 258–270. http://dx.doi.org/10.1016/j.rse.2016.02.060.

White, J.C., Wulder, M.A., Hobart, G.W., Luther, J.E., Hermosilla, T., Griffiths, P., Coops, N.C., Hall, R.J., Hostert, P., Dyk, A., Guindon, L., 2014. Pixel-based image compositing for large-area dense time series applications and science. Can. J. Remote Sens. 40, 192–212. http://dx.doi.org/10.1080/07038992.2014.945827.

White, J.C., Wulder, M.A., Hermosilla, T., Coops, N.C., Hobart, G.W., 2017. Annual characterization of 25 years of forest disturbance and recovery in Canada with

Landsat. Remote Sens. Environ. 194, 303–321. http://dx.doi.org/10.1016/j.rse.2017.03.035.
Williams, C.A., Collatz, G.J., Masek, J., Huang, C., Goward, S.N., 2014. Impacts of disturbance history on forest carbon stocks and fluxes: merging satellite disturbance mapping with forest inventory data in a carbon cycle model framework. Remote Sens. Environ. 151, 57–71. http://dx.doi.org/10.1016/j.rse.2013.10.034.
Wulder, M.A., Coops, N.C., 2014. Make Earth observations open access. Nature 513 (7516), 30–31. http://dx.doi.org/10.1038/513030a.
Wulder, M.A., Kurz, W.A., Gillis, M., 2004. National level forest monitoring and modeling in Canada. Prog. Plann. 61, 365–381.
Wulder, M.A., Masek, J.G., Cohen, W.B., Loveland, T.R., Woodcock, C.E., 2012. Opening the archive: how free data has enabled the science and monitoring promise of Landsat. Remote Sens. Environ. 122, 2–10. http://dx.doi.org/10.1016/j.rse.2012.01.010.
Wulder, M.A., Hilker, T., White, J.C., Coops, N.C., Masek, J.G., Pflugmacher, D., Crevier, Y., 2015. Virtual constellations for global terrestrial monitoring. Remote Sens. Environ. 170, 62–76. http://dx.doi.org/10.1016/j.rse.2015.09.001.
Wulder, M.A., White, J.C., Loveland, T.R., Woodcock, C.E., Belward, A.S., Cohen, W.B., Fosnight, E.A., Shaw, J., Masek, J.G., Roy, D.P., 2016. The global Landsat archive: status, consolidation, and direction. Remote Sens. Environ. 185, 271–283. http://dx.doi.org/10.1016/j.rse.2015.11.032.
Zhu, Z., Woodcock, C.E., 2012. Object-based cloud and cloud shadow detection in Landsat imagery. Remote Sens. Environ. 118, 83–94. http://dx.doi.org/10.1016/j.rse.2011.10.028.
Zhu, Z., Woodcock, C.E., 2014. Automated cloud, cloud shadow, and snow detection in multitemporal Landsat data: an algorithm designed specifically for monitoring land cover change. Remote Sens. Environ. 152, 217–234. http://dx.doi.org/10.1016/j.rse.2014.06.012.
Zhu, Z., Woodcock, C.E., Olofsson, P., 2012. Continuous monitoring of forest disturbance using all available Landsat imagery. Remote Sens. Environ. 122, 75–91. http://dx.doi.org/10.1016/j.rse.2011.10.030.
Zhu, Z., Woodcock, C.E., Holden, C., Yang, Z., 2015. Generating synthetic Landsat images based on all available Landsat data: predicting Landsat surface reflectance at any given time. Remote Sens. Environ. 162, 67–83. http://dx.doi.org/10.1016/j.rse.2015.02.009.
Zhu, Z., 2017. Change detection using Landsat time series: a review of frequencies, preprocessing algorithms, and applications. ISPRS J. Photogramm. Remote Sens. 130, 370–384.